IEEE Access
Multidisciplinary | Rapid Review | Open Access Journal

Received November 4, 2020, accepted November 18, 2020, date of publication November 20, 2020,
date of current version December 7, 2020.

Digital Object Identifier 10.1109/ACCESS.2020.3039636

Impedance-Based Modeling and Common Bus Stability Enhancement Control Algorithm in DC Microgrid

JAE-SUK LEE[1], GI-YOUNG LEE[2], (Member, IEEE), SU-SEONG PARK[1], AND RAE-YOUNG KIM[1], (Senior Member, IEEE)

[1]Department of Electrical and Biomedical Engineering, Hanyang University, Seoul 04763, South Korea
[2]Electric Powertrain R&D Center, Korea Automotive Technology Institute, Cheonan-si 31214, South Korea

Corresponding author: Rae-Young Kim (rykim@hanyang.ac.kr)

This work was supported in part by the "Human Resources Program in Energy Technology" of the Korea Institute of Energy Technology Evaluation and Planning, granted financial resource from the Ministry of Trade, Industry and Energy, Republic of Korea, under Grant 20184010201710, in part by the Korea Electric Power Corporation under Grant R20XO02-4.

ABSTRACT In this paper, impedance modeling of a DC microgrid system consisting of a source and load converter, including an input filter, is performed. Impedance-based modeling has been used to derive mathematical models of the output impedance of the source converter and the input impedance of the load converter. The correlation between the converter interaction and system stability is analyzed based on the mathematical model. An impedance-based stability analysis is used to determine the system stability by analyzing the interactions among the converters in the DC microgrid system. Middlebrook's stability criterion, which uses the impedance transfer function, is applied to determine system stability. Moreover, in this paper, a stability enhancement control algorithm is proposed to resolve the system instabilities resulting from interaction among the converters and the distortion caused by the harmonics emanating from the AC input. The proposed stability enhancement control algorithm consists of a feed-forward type virtual impedance (VI) and a proportional-resonant (PR) controller. The validity of the proposed method is demonstrated by the results of the response characteristics in the frequency domain, and the effectiveness of the proposed control algorithm is verified via simulations and prototype experimental models.

INDEX TERMS DC microgrid, impedance modeling, Middlebrook's stability criterion, stability analysis.

I. INTRODUCTION

In recent years, various studies on precluding environmental pollution caused by the use of petroleum resources and various means of generating self-sufficient electricity using eco-friendly energy resources have been conducted. A DC microgrid system can be self-sufficient in producing electrical energy from renewable energy (e.g., solar and wind) and has the advantage of low power loss because power conversion is not required to use the produced power. Considering these advantages, the system, as mentioned above, has been utilized in buildings, electric ships, and electric vehicles, according to the system size [1]–[4].

A DC microgrid system generally comprises of several converters to connect multiple power sources and loads. These converters are attached through the common bus of the DC microgrid system. To reduce the effect of noise that may be generated by the power generation source on the load, an input filter is placed between the common bus and load converter [5]–[7]. Each converter within a DC microgrid system is generally designed to operate stably. However, when multiple converters operate simultaneously, interactions among them may occur. A converter that operates unstably as a result of these interactions may affect other converters attached to the common bus. Consequently, if the common bus becomes unstable, all the connected converters and the entire DC microgrid system operation may become unstable [5], [8], [9]. Accordingly, it is vital to prepare for this situation to ensure the stable operation of DC microgrid system.

Various stability criteria, such as Middlebrook's stability criterion [10], Gain Margin Phase Margin stability

The associate editor coordinating the review of this manuscript and approving it for publication was Guangdeng Zong.

criterion [11]–[13], and the Passivity-Based stability criterion [14], have been studied to prepare for an unstable DC microgrid system and determine a stable system operation. The criterion for determining the DC microgrid system stability involves classifying the converters comprising the system into the source and load subsystems according to power production and consumption, thereafter, the interactions among these subsystems are analyzed [15], [16]. The Middlebrook's stability criterion and Gain Margin Phase Margin stability criterion classify the converter into the source and load subsystems and determine the stability of the DC microgrid system by analyzing the interactions between the subsystems. The Passivity-Based stability criterion determines stability by reducing the source and load subsystem to a single port network. Among these various stability determination methods, to apply Gain Margin Phase Margin, it is difficult to apply to a system because it is necessary to know both the gain and phase margin of each converter constituting the system [18]. Since the Passivity-Based Stability Criterion combines the source and load subsystems to analyze stability, it is hard to understand the interactions between the source and load subsystems. However, Middlebrook's stability criterion can analyze the interaction between the converters by considering only the gain margin. Stability may be determined by the occurrence of an impedance overlap when the source and load subsystems impedances are indicated in the Bode plot. The occurrence and absence of the impedance overlap between the source and load subsystems indicates that the system is unstable or stable. Therefore, Middlebrook's stability criterion has the advantage of being intuitive because the system stability can be determined by the occurrence of overlapping impedances [13], [17].

As mentioned, if the common bus becomes unstable, the entire system may become unstable. Therefore, DC microgrid system stability analysis consisting of a load converter and input filter is conducted based on a common bus [15], [19]. However, most previous studies have not performed a stability analysis based on the common bus, and only the stability between the input filter and load converter has been examined [20]–[22]. In this case, the interaction analysis between the source and load subsystem based on the common bus may be inaccurate. Consequently, DC microgrid system stability cannot be accurately determined.

In determining stability, the ripple of the common bus increases because of the interaction among the converters comprising the system, thus degrading the system stability. The interaction among converters is caused by the phenomenon of impedance overlap because of the resonance of L and C that comprises the converter. Therefore, the VI control algorithm for reducing the LC resonance is applied to prevent the deterioration of system stability. In [20] and [23], interaction among the converters is reduced by applying VI control algorithm to the part where LC resonance frequency occurs and reinforcing insufficient damping. In this study, the interaction between the LC filter and the load converter is analyzed. In the analysis, the load converter is assumed

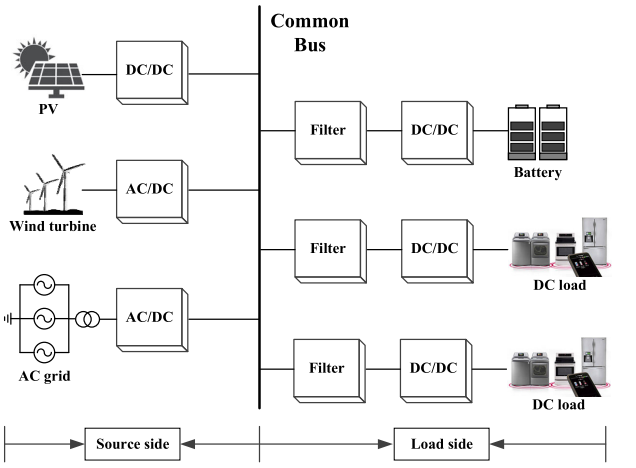

FIGURE 1. Configuration of the DC Microgrid system.

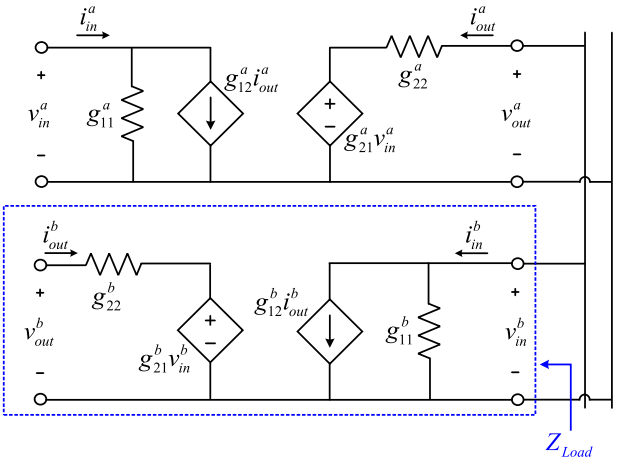

FIGURE 2. Two-port network g-parameter model.

to be Constant Power Load (CPL); hence dynamic characteristics are not considered. Consequently, it is difficult to accurately analyze the DC microgrid system stability. In [24], the system stability analysis is performed by applying the VI control algorithms in series and parallel, considering the dynamic characteristics of the load converter. This method can be used to improve the stability of DC microgrid systems. However, despite the improved system stability through VI, DC microgrid systems should also consider when the AC grid is connected. When an AC grid is connected, harmonics generated at the AC input can distort the current and voltage waveforms. In other words, distorted currents and voltages can adversely affect the common bus, resulting in a decrease in the entire system stability. [25] analyzes the interaction between converters when the input is AC and proposes an impedance shaping method for stable operation. However, the harmonic problem is not considered. Therefore, when the input is AC, a control scheme that can improve the stability considering harmonics is proposed.

In this paper, to more accurately determine the stability of the DC microgrid system, including that of the input filter,

the system stability is determined based on the common bus. Moreover, stability enhancement control algorithm is proposed to reduce the interactions among the converters and eliminate the harmonics generated from the AC input to increase the system stability.

The proposed stability enhancement control algorithm is composed of a feed-forward-type VI and a PR controller. The VI control algorithm reshapes the impedance by adding damping to the resonance frequency to prevent the instability induced by the interaction among the converters because of the overlap in impedance. The PR controller can improve system stability by removing the harmonics [26]. This prevents the system from becoming unstable because of voltage and current distortions induced by the harmonics emanating from the AC input.

The rest of this paper is organized as follows. Section 2 describes the modeling of the impedance of the converters comprising the DC microgrid system. It also presents the derived transfer function of the input and output impedances of the converter. In Section 3, the use of Middlebrook's stability criterion to determine the system stability and converter dynamics is elaborated. Section 4 explains the stability enhancement control algorithm for improving system stability. Section 5 discusses the simulation and experimental verification performed to affirm the corresponding theoretical results. Section 6 summarizes the conclusions of this paper.

II. IMPEDANCE-BASED SYSTEM MODELING FOR STABILITY ANALYSIS

In the DC microgrid system (Figure 1), several converters are attached to the common bus, and the load converter includes an input filter to attenuate the noise component. The interactions among the converters occur when two or more converters are operated [20], [21]. Therefore, it is necessary to understand the cause of the interaction through a stability analysis. In this analysis, a load converter, including a source converter and an input filter, is modeled as input impedance (Z_{in}) and output impedance (Z_{out}) based on the common bus, respectively, as shown in Figure 1 [13].

To perform the system stability analysis through impedance modeling, the two-port network g-parameter model shown in Figure 2 is used [27]. This model can determine the correlation between input and output. Accordingly, the analysis of the interaction among the converters becomes possible. It can also be used when the topology inside the converter is unknown [6], [14].

The g-parameter can express the correlation between the input and output of the converter as (1). The transfer function of the g-parameter is described as (2)–(5) and defined below; g_{11} is the input admittance, g_{21} is the voltage transfer function, g_{12} is the current transfer function, and g_{22} is the output impedance.

$$\begin{bmatrix} I_{in}^a \\ V_{out}^a \end{bmatrix} = \begin{bmatrix} g_{11}^a & g_{12}^a \\ g_{21}^a & g_{22}^a \end{bmatrix} \begin{bmatrix} V_{in}^a \\ I_{out}^a \end{bmatrix} = \mathbf{G} \begin{bmatrix} V_{in}^a \\ I_{out}^a \end{bmatrix} \tag{1}$$

$$g_{11}^a = \frac{1}{Z_{in}} = \left.\frac{i_{in}^a}{v_{in}^a}\right|_{i_{out}^a=0} \tag{2}$$

Using the g-parameter, the input and output transfer functions of one converter is the same as (6). Using this equation, the input and output correlations of the converter may be obtained.

$$g_{12}^a = \left.\frac{i_{in}^a}{i_{out}^a}\right|_{v_{in}^a=0} \tag{3}$$

$$g_{21}^a = \left.\frac{v_{out}^a}{v_{in}^a}\right|_{i_{out}^a=0} \tag{4}$$

$$g_{22}^a = Z_{out} = \left.\frac{v_{out}^a}{i_{out}^a}\right|_{v_{in}^a=0} \tag{5}$$

$$\frac{v_{out}}{v_{in}} = \frac{g_{21}^a}{1+\frac{g_{22}^a}{Z_{Load}}} = \frac{g_{21}^a}{1+\frac{Z_{out}}{Z_{Load}}} \tag{6}$$

Figure 3 is the detailed circuit diagram of the DC microgrid, including the input filter.

By expanding (6), the total transfer function of the system in which the source and load converters are connected (Figure 3) can be calculated and expressed as (7).

$$\frac{v_{L\_out,i}}{v_{s\_in,i}} = \frac{g_{21,\,source}^i g_{21,\,load}^i}{1+\frac{Z_{out,i}}{Z_{in\_f,i}}} \tag{7}$$

where $g_{21,source}^i$ represents the transfer function of the i_{th} source converter, $g_{21,load}^i$ represents the transfer function of the i_{th} load converter and is a fixed value that does not change. Therefore, this fixed value can be omitted, and the equation can be rewritten as (8).

The denominator in (8) can analyze the system stability with the characteristic equation; T_{MLG} indicates the minor loop gain for determining the stability.

$$\frac{v_{L\_out,i}}{v_{s\_in,i}} = \frac{1}{1+\frac{Z_{out,i}}{Z_{in\_f,i}}} = \frac{1}{1+T_{MLG}} \tag{8}$$

The analysis of the interaction among the converters in a DC microgrid system with multiple converters is complex. Accordingly, for a simpler and clearer analysis of the interaction among converters, this paper analyzes the interaction in a system with two converters among those shown in Figure 3. The method of determining the stability by obtaining the impedance of the system is as follows.

The input impedance ($Z_{in,i}(s)$) modeling of the converter can be achieved through $Z_{D,i}(s)$ and $Z_{N,i}(s)$, as (9), (10). $Z_{D,i}(s)$ is the converter input impedance under the condition that $\hat{d}(s)$ is zero, and $Z_{N,i}(s)$ is the value of the converter input impedance under the condition that the controller makes $\hat{v}(s)$ as zero by varying $\hat{d}(s)$.

By substituting (9) and (10) into (11), the input impedance before including the input filter can be obtained.

$$Z_{in,i}(s)\big|_{\hat{d}(s)=0} = Z_{D,i}(s) = \frac{s^2 L_{L,i} C_{L,i} R_{L,i} + s L_{L,i} + R_{L,i}}{D_{L,i}^2 \left(1 + s C_{L,i} R_{L,i}\right)} \tag{9}$$

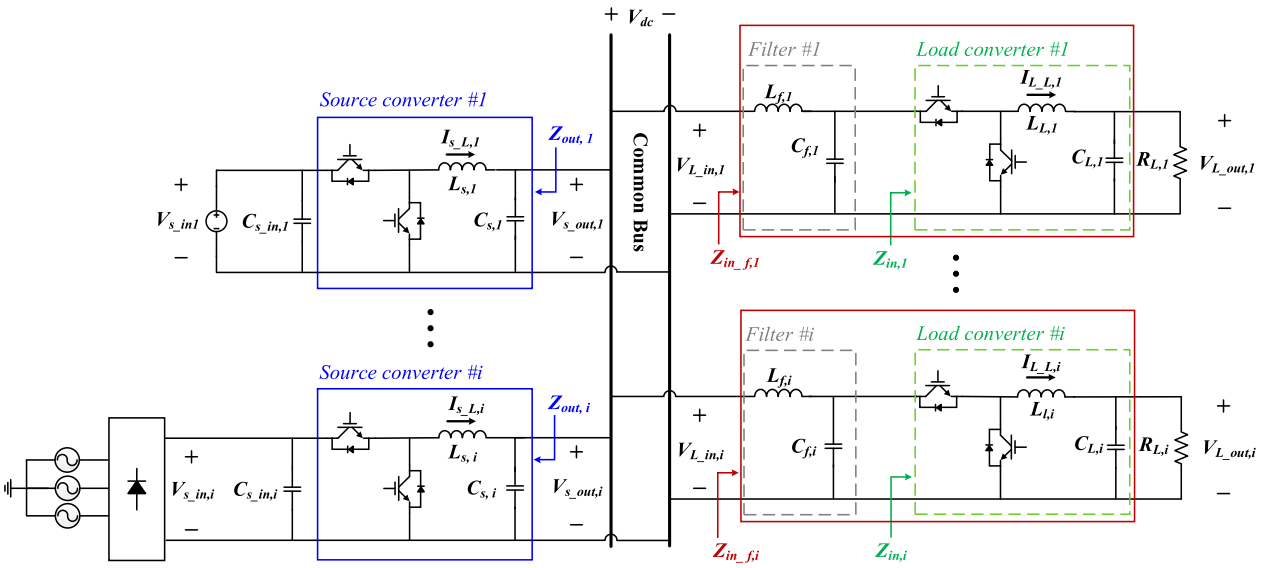

FIGURE 3. DC Microgrid circuit diagram with input filter.

$$Z_{in,i}(s)\big|_{\hat{v}(s)=0} = Z_{N,i}(s) = -\frac{R_{L,i}}{D_{L,i}^2} \tag{10}$$

$$\frac{1}{Z_{in,i}^{CL}(s)} = \frac{1}{Z_{N,i}(s)}\frac{T_{IN}}{1+T_{IN}} + \frac{1}{Z_{D,i}(s)}\frac{1}{1+T_{IN}} \tag{11}$$

The load converter input impedance, including the input filter, can be obtained using (12) and (13), as shown at the bottom of the page, where $Z_{L,i}$ and $Z_{C,i}$ are the impedances of the inductor and capacitor of the input filter, respectively.

The converter impedance, including that of the input filter, can be obtained as (16) using (14) and (15). The load converter loop gain is obtained using (14), and the small- signal open-loop transfer function of the inductor current control is expressed as (15).

$$T_{IN} = H(s)\, C_{load,i}(s)\, G_{id,i}(s)\, G_M \tag{14}$$

$$G_{id,i} = \frac{V_{L\_out,i}\left(1+R_{L,i}C_{L,i}s\right)}{D_{L,i}\left(L_{L,i}C_{L,i}s^2 + L_{L,i}s + 1\right)} \tag{15}$$

$$\frac{1}{Z_{in\_f,i}^{CL}(s)} = \frac{1}{Z_{N\_f,i}(s)}\frac{T_{IN}}{1+T_{IN}} + \frac{1}{Z_{D\_f,i}(s)}\frac{1}{1+T_{IN}} \tag{16}$$

The output impedance ($Z_{out,i}(s)$) can be modeled by the impedance in the direction facing the source converter based on a common bus. When the input voltage variation is zero, the change in the output voltage with respect to the negative variation in load current is the output impedance, as shown in (17).

$$\begin{aligned} Z_{out,i}(s) &= -\left.\frac{\hat{v}_{s\_out,i}(s)}{\hat{i}_{s\_out,i}(s)}\right|_{\substack{\hat{d}=0 \\ \hat{v}_{in}=0}} \\ &= \frac{sL_{s,i}R_{s,i}}{s^2L_{s,i}C_{s,i}R_{s,i} + sL_{s,i} + R_{s,i}} \end{aligned} \tag{17}$$

The output impedance, including that of the controller, can be obtained as (20) using (18) and (19). The source converter loop gain is expressed as (18), and the small-signal open-loop transfer function of the output voltage control is obtained by (19):

$$T_{OUT} = H(s)\, C_{source,i}(s)\, G_{vd,i}(s)\, G_M \tag{18}$$

$$G_{vd,i} = \frac{R_{s,i}V_{s\_out,i}}{D_{s,i}\left(L_{s,i}C_{s,i}R_{s,i}s^2 + L_{s,i}s + R_{s,i}\right)} \tag{19}$$

$$\begin{aligned} Z_{out,i}^{CL}(s) &= \frac{Z_{out,i}(s)}{1+T_{OUT}} \\ &= \frac{sL_{s,i}R_{s,i}}{s^2L_{s,i}C_{s,i}R_{s,i} + sL_{s,i} + R_{s,i}}\frac{1}{1+T_{OUT}} \end{aligned} \tag{20}$$

where $C_{load,i}(s)$, $C_{source,i}(s)$ represents the transfer function of the compensator. $D_{L,i}$, $D_{s,i}$ represents the duty ratio. G_M is

$$\begin{aligned} Z_{D\_f,i}(s) &= Z_{L,i} + \frac{Z_{C,i}Z_{D,i}}{Z_{C,i}+Z_{D,i}} \\ &= sL_{f,i} + \frac{sL_{L,i}\left(1+sC_{L,i}R_{L,i}\right) + R_{L,i}}{s^2C_{f,i}L_{L,i}\left(1+sC_{L,i}R_{L,i}\right) + sC_{f,i}R_{L,i} + D_{L,i}^2\left(1+sC_{L,i}R_{L,i}\right)} \end{aligned} \tag{12}$$

$$Z_{N\_f,i}(s) = Z_{L,i} + \frac{Z_{C,i}Z_{N,i}}{Z_{C,i}+Z_{N,i}} = sL_{f,i} + \frac{R_{L,i}}{D_{L,i}^2 + sC_{f,i}R_{L,i}} \tag{13}$$

the output voltage variation and the pulse width modulation gain according to the function variation of the converter [28], [29]. Stability analysis can be performed on the bode plot using the input and output impedances obtained through impedance- based modeling, and can also be performed by substituting the minor loop gain (21).

$$T_{MLG} = \frac{Z^{CL}_{out,i}(s)}{Z^{CL}_{in\_f,i}(s)} \tag{21}$$

III. SYSTEM STABILITY ANALYSIS

The system stability analysis is conducted using the input impedance obtained by substituting (12) and (13) into (16) and the output impedance of (20). The system for the stability analysis consists of a source converter with an AC power (Figure 3) and a load converter with an input filter. Tables 1 and 2 summarize the parameters for the source and load converters, respectively. Table 3 lists the input filter parameters. The source controller and load converter are designed as type 3 (three-pole and two-zero, respectively). The crossover frequencies of the source and load converters are 110Hz and 380 Hz, respectively.

TABLE 1. System parameters of source converter.

Symbol	Quantity	Value	Unit
P_s	rated power	2	kW
$V_{s\_in,1}$	input voltage	380	V_{ac}
$V_{s\_out,1}$	output voltage	380	V
$L_{s,1}$	inductance	4.3	mH
$C_{s,1}$	capacitance	1000	uF
$C_{s\_in,1}$	input capacitance	10	uF
F_{SW}	switching frequency	10	kHz

TABLE 2. System parameters of load converter.

Symbol	Quantity	Value	Unit
P_L	rated power	2	kW
$V_{L\_in,1}$	input voltage	380	V
$V_{L\_out,1}$	output voltage	190	V
$L_{L,1}$	inductance	1.52	mH
$C_{L,1}$	capacitance	330	uF
F_{SW}	switching frequency	10	kHz

TABLE 3. Input filter parameters

Symbol	Quantity	Value	Unit
$L_{f,1}$	filter inductance	1.5	mH
$C_{f,1}$	filter capacitance	1000	uF

The input and output impedances are present in the bode plot, as shown in Figure 4. Figure 4(a) shows that input and output impedance overlap has occurred. Figure 4(b) shows

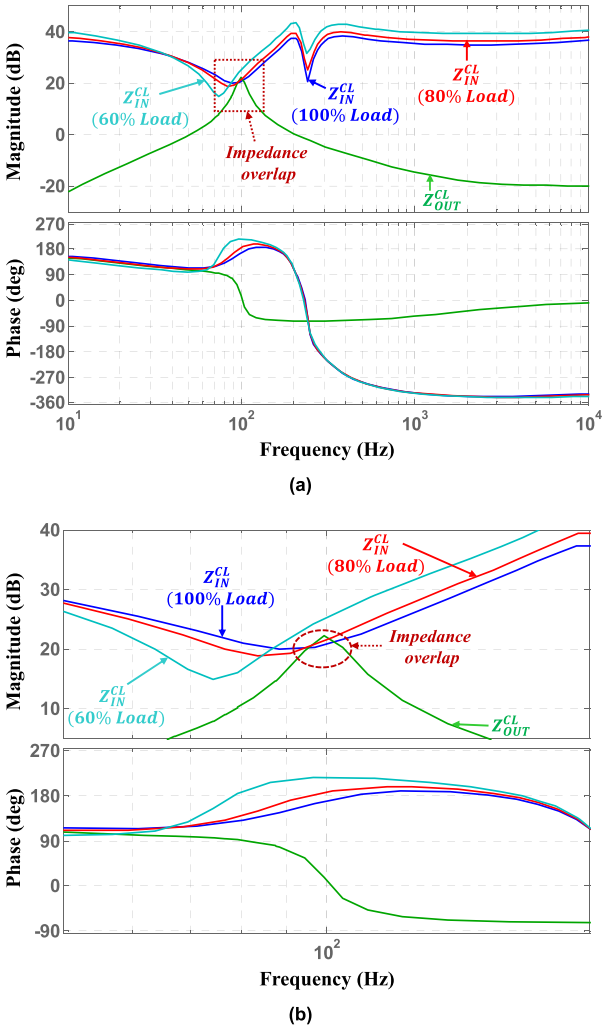

FIGURE 4. System stability analysis (a) Before applying the control algorithm, (b) Enlarged overlap.

this in detail. The impedance overlap does not occur at 60% load, and impedance overlap occurs at above 80% loads.

Middlebrook's stability criterion is applied to this result to determine stability. As mentioned before, Middlebrook's stability criterion considers only the gain margin to determine stability, and the stability criterion is as (22). When the input impedance is less than the output impedance in the frequency range (i.e., input and output impedance overlap), the system is unstable [30], [31].

On the other hand, the system is stable when the input impedance is greater than the output impedance (i.e., input and output impedance overlap does not occur). Therefore, it can be seen that the system is stable at 60% load where input and output impedance overlap does not occur, and the system is unstable at loads above 80% where the impedance overlap occurs. Also, stability can be determined using the Nyquist contour T_{MLG}. If the Nyquist contour is inside the unit circle, the system is stable, and if it is located in the forbidden region outside the unit circle, the system is unstable [30]. Nyquist contour can be obtained using (22) and is shown in Figure 5.

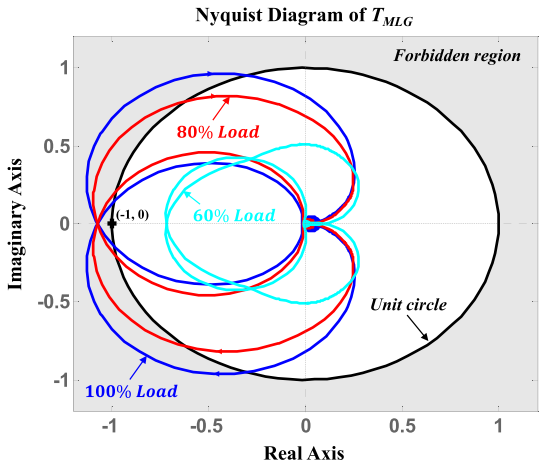

FIGURE 5. Nyquist diagram before applying the control algorithm.

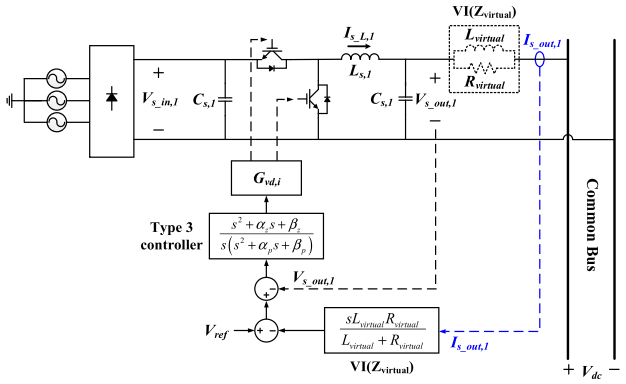

FIGURE 6. Applying VI control algorithm block diagram.

In Figure 5, at 60% load, the Nyquist contour is inside the unit circle and does not contain (-1,0), so the system is stable. On the other hand, at loads above 80%, the Nyquist contour leaves the unit circle and enters the forbidden area, and the system is unstable because it contains (-1,0). Therefore, a control algorithm is required to improve the system stability at this unstable load.

$$\|T_{MLG}\| = \left\| \frac{Z_{out,i}^{CL}}{Z_{in,i}^{CL}} \right\| \ll 1 \ : \ \text{stable}$$
$$\|T_{MLG}\| = \left\| \frac{Z_{out,i}^{CL}}{Z_{in,i}^{CL}} \right\| \gg 1 \ : \ \text{unstable} \qquad (22)$$

IV. STABILITY ENHANCEMENT CONTROL SCHEME

Impedance reshaping is required to satisfy Middlebrook's stability criterion and improve the stability of the system. In this process, the input and output impedances are reshaped by modifying or changing the controllers of the source and load converters. In this paper, the output converter impedance is reshaped by modifying the controller of the source converter to avoid the impedance overlap. To reshape the output impedance, VI control algorithm is applied between the source converter and the common bus, as shown in Figure 6.

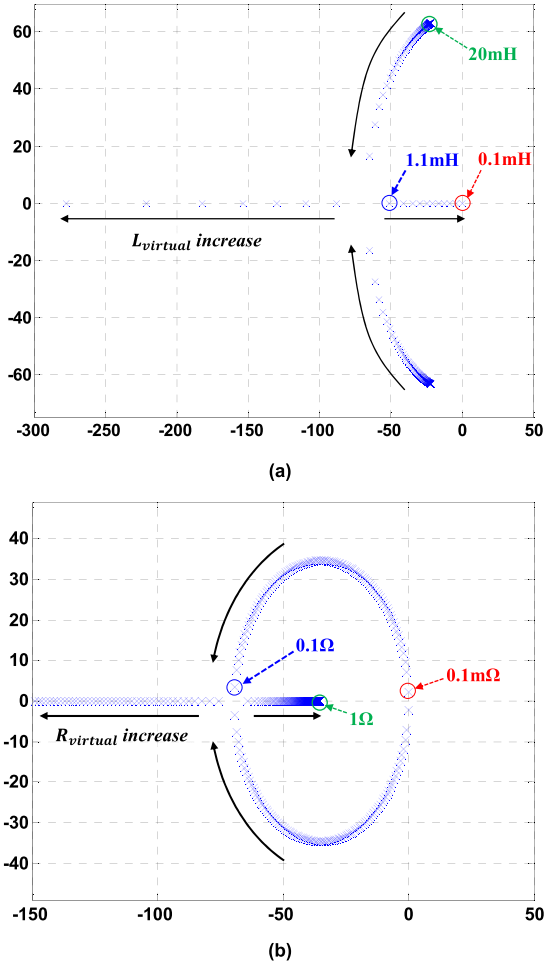

FIGURE 7. Eigenvalue changes according to the $L_{virtual}$ and $R_{virtual}$ (a) $L_{virtual}$, (b) $R_{virtual}$.

The VI is added to the existing control block diagram to perform the same behavior as the dotted line circuit. By adding a VI, the output impedance is reshaped at frequencies where impedance overlap occurs due to insufficient damping in the source converter [32], [33]. Thus, it can meet Middlebrook's stability criterion and stabilize the system. VI is expressed as (23). The output impedance, including the VI, is expressed as (24).

$$Z_{virtual} = \frac{sL_{virtual}R_{virtual}}{L_{virtual} + R_{virtual}} \qquad (23)$$

$$Z_{out\_virtual}^{CL} = \frac{Z_{virtual}Z_{out}^{CL}}{(1 + T_{OUT})\left(Z_{virtual} + Z_{out}^{CL}\right)} \qquad (24)$$

VI is applied to eliminate impedance overlap due to a lack of damping. Therefore, by analyzing the Eigenvalue of the controller, including the VI, the value with the largest damping effect (i.e., the pole of the left half plane far from the origin) is selected. The two scenarios are implemented for the selected impedance values. In the first scenario, the virtual resistance is fixed at 1 Ω, and the virtual inductance fluctuates between 0.1 and 20 mH. In the second scenario, the virtual inductance is fixed at 1 mH, and the virtual resistance fluctuates from 0.1 mΩ to 1 Ω. Figure 7 (a) presents

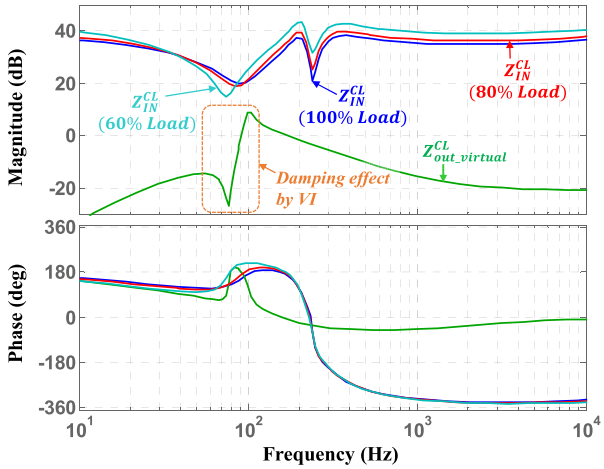

FIGURE 8. System stability analysis with VI control algorithm.

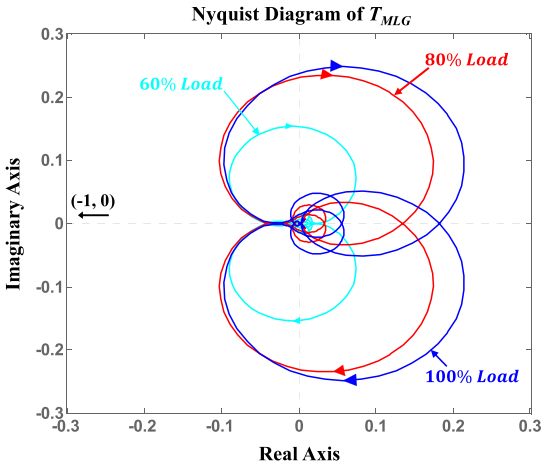

FIGURE 9. Nyquist diagram with VI control algorithm.

the Eigenvalue waveform when the first scenario is implemented. At 0.1 mH, the pole of the system is located at the boundary between the right-half plane (RHP) and the left-half plane (LHP). Figure 7 (b) presents the Eigenvalue waveform when the second scenario is implemented. When the virtual resistance value is small, the pole of the system approaches the boundary between RHP and LHP. As the pole of the system approaches the RHP, the damping ratio of the system decreases, and the system may become unstable.

So, for stable operation with a high damping ratio, choose a pole far from the RHP as follows: The virtual inductance value is 1.1mH, and the virtual resistance value is 0.1 Ω.

The Bode plot waveform when the VI control algorithm is applied using the selected VI value is shown in Figure 8. It can be confirmed from the figure that the impedance overlap is eliminated because of the additional damping effect, thus implying the system is stable because it satisfies Middlebrook's stability criterion. The Nyquist diagram where the VI control algorithm is applied is shown in Figure 9; the Nyquist

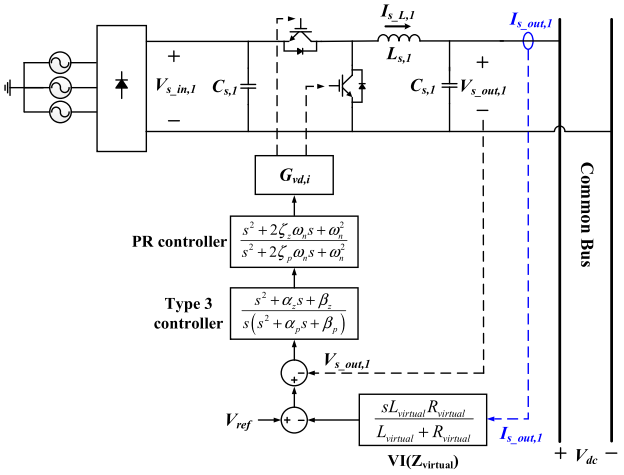

FIGURE 10. Proposed enhancement control algorithm block diagram.

diagram does not contain $(-1, 0)$, referring that the system is stable.

The system is stabilized through the VI control algorithm, but in the case of DC microgrid system, the AC power source is connected as mentioned above. The harmonics generated by the AC power source can affect the stability of the entire system. Therefore, additional control algorithm is necessary to prevent the degradation caused by these harmonics. In this paper, as shown in Figure 10, the system stability degradation is prevented by using a stability enhancement controller that adds a PR controller to the existing VI controller. The PR control can reduce the influence of harmonics by increasing the size of a specific frequency preferred by the designer without significantly changing the steady-state error and the system stability on the existing controller [34]. The PR controller applied in this paper is expressed as (25). The AC input and diode rectifier are used to simulate the AC power source simply.

In Equation (25), ω_n is a value employed to reduce the 6th and 12th harmonics (i.e., 360Hz and 720Hz harmonics, respectively) generated after passing through the diode rectifier. The magnitude at a specific frequency can be varied by setting ζ_z and ζ_p. The loop gain with the PR controller added is as in (26). Using this, the output impedance can be calculated as (27).

$$C_{PR} = \frac{s^2 + 2\zeta_z\omega_n s + \omega_n^2}{s^2 + 2\zeta_p\omega_n s + \omega_n^2} \tag{25}$$

$$T_{PR} = H(s)\, C_{source}(s)\, C_{PR}(s)\, G_{vd}(s)\, G_M \tag{26}$$

$$Z_{out\_PR}^{CL} = \frac{Z_{virtual} Z_{out}^{CL}}{(1 + T_{PR})\left(Z_{virtual} + Z_{out}^{CL}\right)} \tag{27}$$

Figure 11 presents the analysis waveform after applying the stability enhancement control algorithm and adding the VI and PR controllers to the existing controller. The impedance overlap is eliminated because of the additional damping effect by applying VI; the loop gain at the specific frequency increases when the PR controller is added.

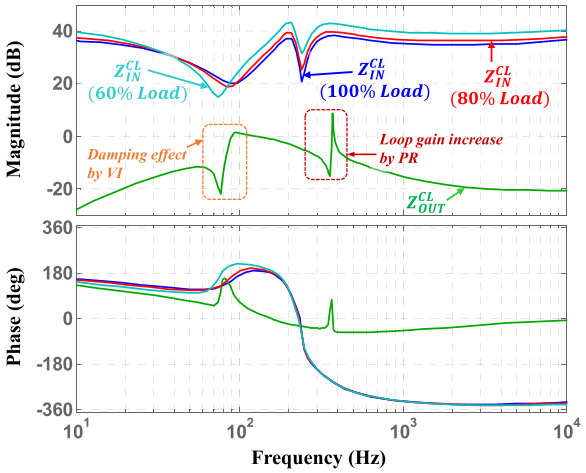

FIGURE 11. System stability analysis applying proposed stability enhancement control algorithm (VI with PR).

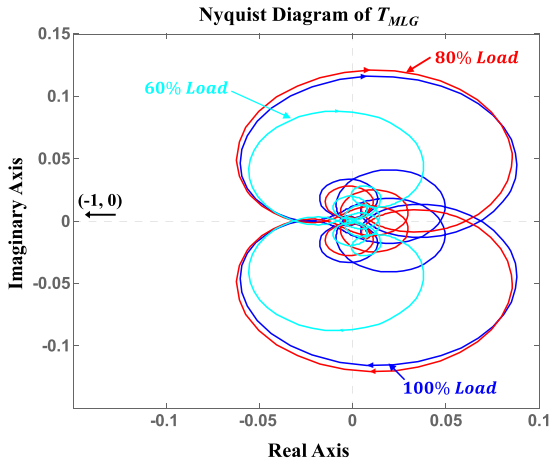

FIGURE 12. Nyquist diagram with enhancement control algorithm (VI with PR).

Thus, it can reduce harmonics. Moreover, even if the PR controller is added (Figure 12), it can be confirmed through the Nyquist diagram that the system is stable. Before the proposed control algorithm is applied, the system is unstable because the Nyquist diagram is including (-1, 0) (Figure 5). However, when the proposed stability enhancement algorithm is applied, the system becomes stable, as indicated by the absence of (−1, 0) in the Nyquist diagram (Figure 12). The proposed stability enhancement algorithm reduced the interaction among the converters and reduced the harmonics, improved system stability.

V. SIMULATION AND EXPERIMENTAL RESULTS

A. SIMULATION RESULTS

To verify the performance of the aforementioned stability enhancement control algorithm, a simulation is performed by configuring a circuit with a source converter with AC power input and a load converter, including input filter, as shown in Figure 3. Tables 1−3 summarize the system parameter details. The simulations are performed at 60%, 80%, and 100% load conditions. Figure 13 depicts a waveform before the stability enhancement algorithm is applied. The stability analysis in Figure 4 shows that the system is stable because an impedance overlap does not occur at the 60% load. In contrast, the system is unstable because of the impedance overlap when the load is 80% or more load.

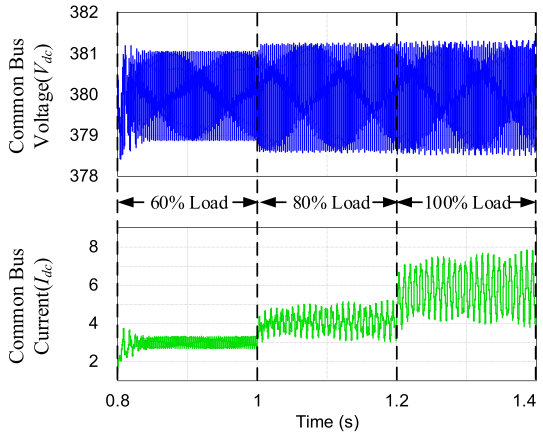

FIGURE 13. Simulation results of load change before applying control algorithm.

Based on the analysis, the simulation results in Figure 13 exhibit a stable waveform that does not increase or distort the ripple at the 60% load. However, the figure also shows that the ripple increases and distortion occurs in the waveform when the impedance overlap occurs at 80% or more of the load. Figure 14 (a) exhibits an enlarged waveform of the 80% load waveform presented in Figure 13. Based on the analysis, the system became unstable at loads above 80% due to the overlap of the input and output impedances and the harmonics occurring at the AC input. Figure 14(b) is a simulation waveform when the VI control algorithm is applied. Based on the waveform, the ripple value decreases from 2.1 A to 0.95 A. Moreover, the distorted waveform becomes smoother than before the control algorithm is applied; nevertheless, the waveform is still distorted due to harmonics. Figure 14(c) shows the simulation waveform when the proposed enhancement control algorithm is applied. The ripple is further reduced compared to when only the VI control algorithm is applied; the ripple decreases from 2.1 to 0.7 A. Moreover, it can be confirmed that the phenomenon in which the waveform is distorted because of the harmonics does not occur. Accordingly, the effective performance of the proposed control algorithm is confirmed.

B. EXPERIMENTAL RESULTS

Figure 15 shows the experimental equipment used to conduct the aforementioned analysis and verify the effectiveness of the proposed stability enhancement control algorithm. The experimental equipment parameters are the same as those specified in Section 3.

The experimental conditions are compared when the control algorithm is not applied under the 80% load condition where the system becomes unstable, when the VI control algorithm is applied, and when the proposed stability

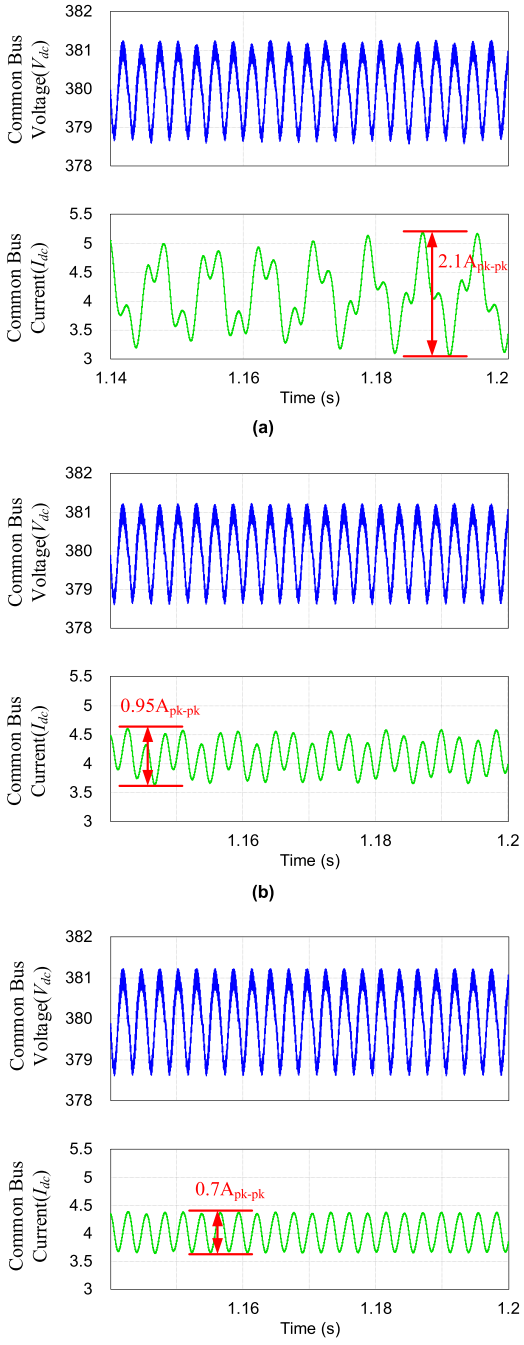

FIGURE 14. Simulation results (a) Before applying control algorithm (b) VI control algorithm (c) Enhancement control algorithm.

enhancement control algorithm is applied. Before applying, the control algorithm in the previous analysis has confirmed that the impedance overlap occurs by the interaction between the converters. Therefore, the waveform of Figure 16 (a), it can confirm that the current and voltage ripple of the common bus has a large ripple and a distorted waveform similar to the simulation result. The experimental result of applying the VI control algorithm is shown in Figure 16(b). Based on the resulting waveform, the current ripple is reduced to 2.4 A from 3 A, and the voltage ripple is reduced to 8.8 V from 10 V. Moreover, it can be observed that the distortion

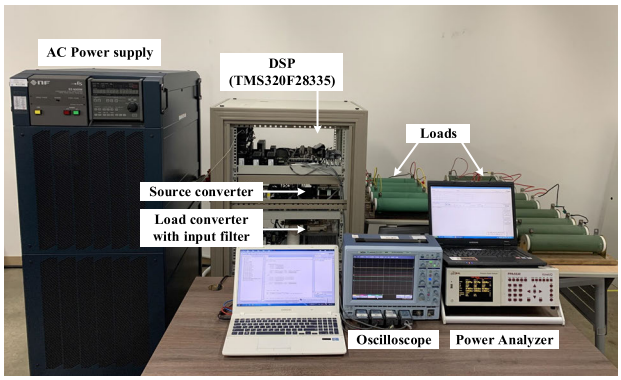

FIGURE 15. Experimental equipment.

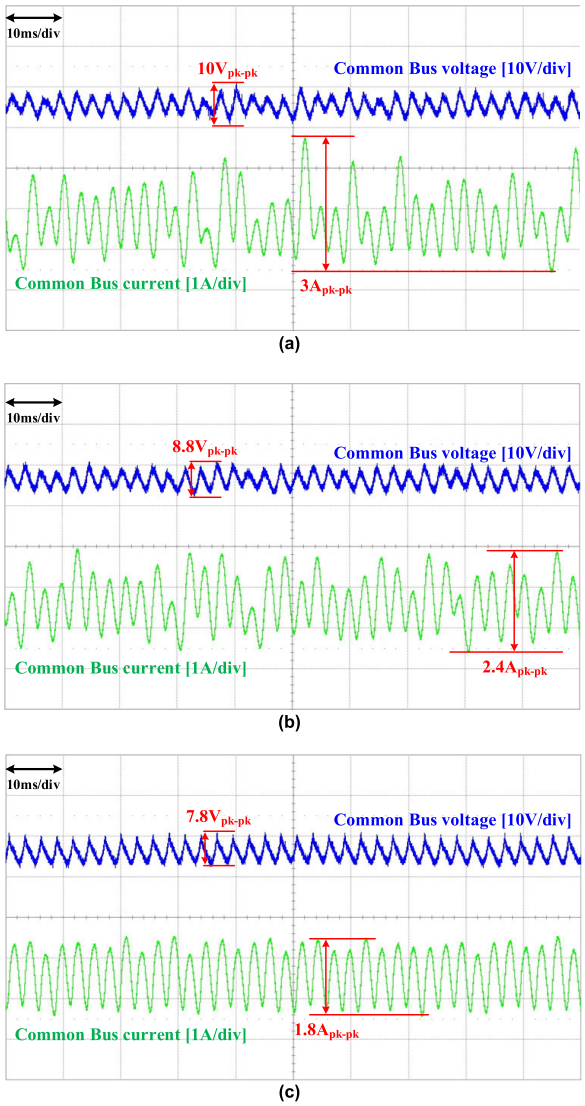

FIGURE 16. Experimental results (a) Before applying control algorithm (b) VI control algorithm (c) Enhancement control algorithm.

of the waveform has a smooth change and is relatively stable. However, it is confirmed that the ripple value remains high, and waveform distortions still exist. Therefore, it is necessary to stabilize the common bus by suppressing the ripple in

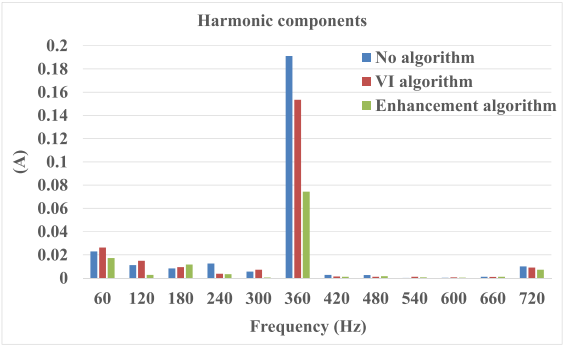

FIGURE 17. Harmonic analysis using a power analyzer.

TABLE 4. Total harmonic distortion value of the common bus.

Frequency (Hz)	No algorithm	VI algorithm	Enhancement algorithm
60	0.023	0.02627	0.01717
120	0.01109	0.01484	0.00272
180	0.00827	0.00941	0.0116
240	0.01254	0.0037	0.00337
300	0.00555	0.00711	0.00046
360	0.19107	0.15345	0.07443
420	0.00267	0.00132	0.00117
480	0.00258	0.0011	0.0016
540	0.00003	0.00116	0.00052
600	0.00025	0.00066	0.00036
660	0.0011	0.00092	0.00101
720	0.01001	0.00902	0.00726

the common bus resulting from the interaction among the converters and reducing the voltage and current distortion caused by the harmonics included in the AC input. In this paper, stability enhancement control algorithm that is more robust than the VI control algorithm is applied. The waveform to which the stability enhancement control algorithm is applied is shown in Figure 16 (c). The figure indicates that when the stability enhancement control algorithm is applied, the current ripple is reduced to 1.8 A from 2.4 A. The voltage ripple further reduces to 7.8 V from 8.8 V compared to that when only the existing VI control algorithm is applied. Moreover, the waveform distortion caused by harmonics is almost eliminated, and a stable waveform can be confirmed. This paper verified whether the influence of the input harmonics on the common bus is reduced by the proposed stability enhancement control algorithm using the power analyzer. The analysis results are the same as those in Figure 17, and the harmonic values are summarized in Table 4. The analysis results indicate that the harmonics are generally reduced when the proposed stability enhancement control algorithm is applied compared with that when only the VI control algorithm is used. In particular, at 360 Hz, the harmonics are reduced by 60% when applying the control algorithm.

VI. CONCLUSION

In this paper, a control algorithm for the enhancement stability of the DC microgrid system is proposed. Impedance-based modeling was performed for the DC microgrid system stability analysis, including input filters. The stability analysis was conducted based on the DC bus. The interactions among the converters that occur when the DC microgrid system operates are analyzed through the aforementioned impedance-based modeling. Then, the stability enhancement control algorithm is proposed to overcome the system instability, determined through the analysis. The proposed stability enhancement control algorithm reshaped the output impedance by adding the VI of the source converter to prevent stability degradation results from the interaction among the converters, thereby avoiding the overlap between the input and output impedances. This reshaping can suppress the interaction among the converters. Moreover, the system stability is improved using the PR control to reduce the unstable effect (i.e., voltage and current distortion) of AC input harmonics on the system. The proposed stability enhancement control algorithm is verified by implementing a simulation and an experiment using the prototype experimental equipment. Finally, it is confirmed that the proposed enhancement control algorithm has improved system stability by reducing the ripple and harmonics of the common bus.

REFERENCES

[1] F. Gao and S. Bozhko, "Modeling and impedance analysis of a single DC bus-based multiple-source multiple-load electrical power system," *IEEE Trans. Transport. Electrific.*, vol. 2, no. 3, pp. 335–346, Sep. 2016.

[2] Q. Xu, C. Zhang, C. Wen, and P. Wang, "A novel composite nonlinear controller for stabilization of constant power load in DC microgrid," *IEEE Trans. Smart Grid*, vol. 10, no. 1, pp. 752–761, Jan. 2019.

[3] A. Aldhaheri and A. Etemadi, "Impedance decoupling in DC distributed systems to maintain stability and dynamic performance," *Energies*, vol. 10, no. 4, p. 470, Apr. 2017.

[4] A. A. Saad, S. Faddel, T. Youssef, and O. Mohammed, "Small-signal model predictive control based resilient energy storage management strategy for all electric ship MVDC voltage stabilization," *J. Energy Storage*, vol. 21, pp. 370–382, Feb. 2019.

[5] M. Wu and D. D.-C. Lu, "A novel stabilization method of LC input filter with constant power loads without load performance compromise in DC microgrids," *IEEE Trans. Ind. Electron.*, vol. 62, no. 7, pp. 4552–4562, Jul. 2015.

[6] S. Vesti, J. A. Oliver, R. Prieto, J. A. Cobos, J. Huusari, and T. Suntio, "Practical characterization of input-parallel-connected converters with a common input filter," in *Proc. 27th Annu. IEEE Appl. Power Electron. Conf. Expo. (APEC)*, Orlando, FL, USA, Feb. 2012, pp. 1845–1852.

[7] R. Ahmadi and M. Ferdowsi, "Modeling closed-loop input and output impedances of DC-DC power converters operating inside DC distribution systems," in *Proc. IEEE Appl. Power Electron. Conf. Expo. (APEC)*, Fort Worth, TX, USA, Mar. 2014, pp. 1131–1138.

[8] X. Li, X. Ruan, X. Xiong, Q. Jin, and C. K. Tse, "Stability issue of cascaded systems with consideration of switching ripple interaction," *IEEE Trans. Power Electron.*, vol. 34, no. 7, pp. 7040–7052, Jul. 2019.

[9] L. Guo, S. Zhang, X. Li, Y. W. Li, C. Wang, and Y. Feng, "Stability analysis and damping enhancement based on frequency-dependent virtual impedance for DC microgrids," *IEEE J. Emerg. Sel. Topics Power Electron.*, vol. 5, no. 1, pp. 338–350, Mar. 2017.

[10] R. D. Middlebrook, "Input filter consideration in design and application of switching regulators," in *Proc. IEEE IAS*, May 1976, pp. 366–382.
[11] X. Feng, J. Liu, and F. C. Lee, "Impedance specifications for stable DC distributed power systems," *IEEE Trans. Power Electron.*, vol. 17, no. 2, pp. 157–162, Mar. 2002.
[12] C. M. Wildrick, F. C. Lee, B. H. Cho, and B. Choi, "A method of defining the load impedance specification for a stable distributed power system," *IEEE Trans. Power Electron.*, vol. 10, no. 3, pp. 280–285, May 1995.
[13] A. Riccobono and E. Santi, "Comprehensive review of stability criteria for DC power distribution systems," *IEEE Trans. Ind. Appl.*, vol. 50, no. 5, pp. 3525–3535, Sep. 2014.
[14] J. Siegers, S. Arrua, and E. Santi, "Stabilizing controller design for multi-bus MVdc distribution systems using a passivity-based stability criterion and positive feedforward control," *IEEE J. Emerg. Sel. Topics Power Electron.*, vol. 5, no. 1, pp. 14–27, Mar. 2017.
[15] X. Wang, Y. Peng, J. Zhu, Y. Xia, M. Yu, H. Hu, H. Cai, and W. Wei, "Decentralized impedance specifications for small-signal stability of DC distributed power systems," *IEEE J. Emerg. Sel. Topics Power Electron.*, vol. 5, no. 4, pp. 1578–1588, Dec. 2017.
[16] A. Riccobono and E. Santi, "Stability analysis of an all-electric ship MVDC power distribution system using a novel passivity-based stability criterion," in *Proc. IEEE Electr. Ship Technol. Symp. (ESTS)*, Arlington, VA, Apr. 2013, pp. 411–419.
[17] A. Riccobono, M. Cupelli, A. Monti, E. Santi, T. Roinila, H. Abdollahi, S. Arrua, and R. A. Dougal, "Stability of shipboard DC power distribution: Online impedance-based systems methods," *IEEE Electrific. Mag.*, vol. 5, no. 3, pp. 55–67, Sep. 2017.
[18] J. Yang, G. Buticchi, C. Gu, S. Gunter, H. Zhang, and P. Wheeler, "A generalized input impedance model of multiple active bridge converter," *IEEE Trans. Transport. Electrific.*, vol. 6, no. 4, pp. 1695–1706, Dec. 2020, doi: 10.1109/TTE.2020.2986604.
[19] A. Aldhaheri and A. Etemadi, "Mitigating the impedance-based interaction in DC distributed power systems," in *Proc. IEEE Power Energy Conf. Illinois (PECI)*, Chicago, IL, USA, Feb. 2018, pp. 1–5.
[20] M. Wu, D. D.-C. Lu, and C. K. Tse, "Direct and optimal linear active methods for stabilization of LC input filters and DC/DC converters under voltage mode control," *IEEE J. Emerg. Sel. Topics Circuits Syst.*, vol. 5, no. 3, pp. 402–412, Sep. 2015.
[21] X. Huang, Z. He, Z. Chen, Y. Liu, W. Wu, Q. Xu, L. Zhou, and A. Luo, "Stability assessment and coordinated impedance shaping strategy for DC bidirectional cascaded system with LC input filter," *Int. J. Electr. Power Energy Syst.*, vol. 115, Feb. 2020, Art. no. 105429.
[22] M. N. Hussain and V. Agarwal, "A novel feedforward stabilizing technique to damp power oscillations caused by DC–DC converters fed from a DC bus," *IEEE J. Emerg. Sel. Topics Power Electron.*, vol. 8, no. 2, pp. 1528–1535, Jun. 2020.
[23] M. N. Hussain, R. Mishra, and V. Agarwal, "A self-switched virtual impedance based stabilization method for a droop controlled DC microgrid with constant power loads and input load filters," in *Proc. IEEE Int. Conf. Power Electron., Drives Energy Syst. (PEDES)*, Trivandrum, Kerala, Dec. 2016, pp. 1–6.
[24] X. Zhang, X. Ruan, and Q.-C. Zhong, "Improving the stability of cascaded DC/DC converter systems via shaping the input impedance of the load converter with a parallel or series virtual impedance," *IEEE Trans. Ind. Electron.*, vol. 62, no. 12, pp. 7499–7512, Dec. 2015.
[25] F. Feng, F. Wu, and H. B. Gooi, "Impedance shaping of isolated two-stage AC-DC-DC converter for stability improvement," *IEEE Access*, vol. 7, pp. 18601–18610, 2019.
[26] K. Lim and J. Choi, "PR control based cascaded current and voltage control for seamless transfer of microgrid," in *Proc. IEEE 2nd Int. Future Energy Electron. Conf. (IFEEC)*, Taipei, Taiwan, Nov. 2015, pp. 1–6.
[27] C. K. Alexander and M. Sadiku, *Fundamental of Electric Circuits*, 5th ed. New York, NY, USA: McGraw-Hill, 2013.
[28] R. W. Erickson and D. Maksimovic, *Fundamentals of Power Electronics*, 2nd ed. New York, NY, USA: Springer, 2001.
[29] R. Ahmadi, D. Paschedag, and M. Ferdowsi, "Analyzing stability issues in a cascaded converter system comprised of two voltage-mode controlled DC-DC converters," in *Proc. 26th Annu. IEEE Appl. Power Electron. Conf. Expo. (APEC)*, Fort Worth, TX, USA, Mar. 2011, pp. 1769–1775.
[30] S. Singh, A. R. Gautam, and D. Fulwani, "Constant power loads and their effects in DC distributed power systems: A review," *Renew. Sustain. Energy Rev.*, vol. 72, pp. 407–421, May 2017.
[31] Z. Jin and J. M. Guerreros, "Two-degree-of-freedom admittance-type droop control for plug-and-play DC microgrid," in *Proc. IEEE Appl. Power Electron. Conf. Expo. (APEC)*, San Antonio, TX, USA, Mar. 2018, pp. 3326–3332.
[32] X. Zhang, Q.-C. Zhong, V. Kadirkamanathan, J. He, and J. Huang, "Source-side series-virtual-impedance control to improve the cascaded system stability and the dynamic performance of its source converter," *IEEE Trans. Power Electron.*, vol. 34, no. 6, pp. 5854–5866, Jun. 2019.
[33] M. N. Hussain, R. Mishra, and V. Agarwal, "A frequency-dependent virtual impedance for voltage-regulating converters feeding constant power loads in a DC microgrid," *IEEE Trans. Ind. Appl.*, vol. 54, no. 6, pp. 5630–5639, Nov. 2018.
[34] M. Castilla, "Linear current control scheme with series resonant harmonic compensator for single-phase grid-connected photovoltaic inverters," *IEEE Trans. Ind. Electron.*, vol. 55, no. 7, pp. 2724–2733, Jul. 2008.

JAE-SUK LEE received the B.S. degree in electrical engineering from Kookmin University, Seoul, South Korea, in 2015. He is currently pursuing the Ph.D. degree with the Energy Power Electronics Control System Laboratory, Hanyang University, Seoul, South Korea. His research interests include control of distributed power converter systems, renewable energy, and microgrid.

GI-YOUNG LEE (Member, IEEE) received the B.S. and Ph.D. degrees in electrical engineering from Hanyang University, Seoul, South Korea, in 2013 and 2019, respectively. In 2019, he was a Senior Researcher with LSIS Company, South Korea. Since 2019, he has been with the Korea Automotive Technology Institute, Cheonan-si, South Korea, where he is currently a Senior Researcher with the Electric Powertrain R&D Center. His current research interests include modeling and control of distributed power conversion systems, converters for renewable energies, microgrids, power converters for electric vehicle, and motor drives.

SU-SEONG PARK received the B.S. degree in electrical engineering from Hanyang University, Seoul, South Korea, in 2020, where he is currently pursuing the Ph.D. degree with the Energy Power Electronics Control System Laboratory. His research interests include control of distributed power converter systems, renewable energy, and microgrid.

RAE-YOUNG KIM (Senior Member, IEEE) received the B.S. and M.S. degrees from Hanyang University, Seoul, South Korea, in 1997 and 1999, respectively, and the Ph.D. degree from Virginia Polytechnic Institute and State University, Blacksburg, VA, USA, in 2009, all in electrical engineering.

From 1999 to 2004, he was a Senior Researcher with the Hyosung Heavy Industry R&D Center, Seoul, South Korea. In 2009, he was a Postdoctoral Researcher with National Semiconductor Corporation, Santa Clara, CA, USA, involved in a smart home energy management system. In 2016, he was a Visiting Scholar with the Center for Power Electronics Systems (CPES), Virginia Polytechnic Institute and State University, Blacksburg. Since 2010, he has been with Hanyang University, where he is currently an Associate Professor with the Department of Electrical and Biomedical Engineering. His research interests include the design of high power density converters and the distributed control of power converters for modular power converter systems in the applications of renewable energy, wireless power transfer, micro grid, and motor drive.

Dr. Kim was a recipient of the 2007 First Prize Paper Award from the IEEE IAS.